Automated Blood Vessel Segmentation in Fundus Image Based on Integral Channel Features and Random Forests

Zhun Fan, Yibiao Rong, Jiewei Lu, Jiajie Mo, Fang Li, Xinye Cai and Tiejun Yang

Abstract— Automated detection of blood vessel structures is becoming a crucial interest for better management of vascular disease. In this paper, we propose an algorithm for vessel segmentation in digital retinal images based on integral channel features and random forests. In the first stage, preprocessing is performed to obtain the candidate pixels of vessels, then a host of simple features are extracted for each candidate pixels based on integral channels. Furthermore random forests is used to classify the candidate pixels as vessels or not. Finally, postprocessing is applied to fill pixel gaps in classified blood vessels. The proposed algorithm achieves an average accuracy of 0.9614, 0.9588, sensitivity of 0.7191, 0.6996 and specificity of 0.9849, 0.9787 on two public databases DRIVE and STARE respectively.

I. INTRODUCTION

ANALYSIS of the retinal blood vessels from fundus images has been widely used by medical community for diagnosing complications due to hypertension, arteriosclerosis, cardiovascular disease, glaucoma, stroke and diabetic retinopathy[1]. However, as the increasing of the patients with eye diseases, the number of ophthalmologists needed for evaluation by direct examination becomes a huge limiting factor for hospitals. As a result, an automated blood vessels segmentation algorithm is desired.

Many vessel segmentation algorithms have been introduced in the literatures, which can be divided into 7 categories: 1) pattern recognition techniques[4,8,9], 2) matched filtering[26,27], 3) vessel tracking / tracing[28], 4) mathematical morphology[16,29], 5) multi-scale approaches[30,31], 6) model based approaches[18,20] and 7) parallel / hardware based approaches[2]. The pattern recognition techniques can be further divided into two subcategories: supervised approaches and unsupervised approaches. Since supervised methods are designed based on pre-classified data, their performance is usually better than that of unsupervised ones[2]. Therefore, supervised methods for vessel segmentation is utilized most frequently among these methods.

The performance of supervised method is determined by two key factors: the learning algorithm and the feature

Zhun Fan, Yibiao Rong, Jiewei Lu, Jiajie Mo and Fang Li are with the Department Electrical Information Engineering, Shantou University, Shantou, GuangDong (email: {zfan, 13ybrong, 12jwlu1, 12jjmo, 13fli}@stu.edu.cn); Xinye Cai is with the Department of Computer Science and Technology, Nanjing University of Aeronautics and Astronautics, Nanjing(email: {xinye}@nuaa.edu.cn); Tiejun Yang is with the Guilin University of Technology, Guilin, Guangxi(email: {yattie}@126.com)

representation. For vessel segmentation, many researchers utilized off-the-shelf learning algorithms directly and poured attention into the design of feature representation. For example, in [3], E. Ricci et al. employed two orthogonal line detectors along with the grey level of the target pixel to construct a feature vector for supervised classification using support vector machine. D. Marin et al. [4] computed a 7-D vector composed of gray-level and moment invariants-based features for pixel representation and used a neural network scheme for pixel classification. S. Roychowdhury et al. [1] employed a classifier of gaussian mixture model using a set of 8 features that are extracted based on the neighborhood of the pixel and its first and second-order gradients for pixel classification.

Although promising performance can be achieved using hand-tuned features, the disadvantages of hand-tuned features are obvious, such as, requiring expert knowledge, being time-consuming and difficult to be generalized to other domains.

To alleviate the burden of manual feature design for vessel segmentation, we propose an algorithm based on integral channel features and random forests in this paper. The inspiration of the proposed method comes from [5], where integral channel features are computed using linear and non-linear transformations of the input image. Since the transformations are simple, the human effort on feature design is minimized. To represent the target pixel, we use a small patch which centers on the target pixel to construct a feature vector on each channel. Thus, abundant features for each pixel can be obtained. To avoid the process of feature selection, random forests, which deals well with high dimensional data, is chosen as the classifier in this work.

The proposed algorithm has been evaluated on the publicly available STARE[6] and DRIVE[7] databases. The averagely obtained values (sensitivity of 0.7191, specificity of 0.9849, accuracy of 0.9614 on DRIVE database, and 0.6996, 0.9787, 0.9588 on STARE database) show that the proposed method is an effective tool for vessel segmentation. The experimental results also demonstrate that the proposed method is very competitive with the state-of-the-art methods, such as [3,4,6,8,9].

The rest of this paper is organized as follows: Section II describes the public databases used in this study. Section III explains and illustrates the proposed method for vessel segmentation. Section IV shows the experimental results obtained using the public databases, and a comparison study with other methods from the literatures. We provide discussions and conclusions in Section V.

II. PUBLIC DATABASES

In order to evaluate the vessel segmentation methodology, two publicly available databases containing retinal images, the DRIVE[7] and STARE[6] databases, were used. These two databases have been widely used by other researchers to test their vessel segmentation methodologies since they provide manual segmentations for performance evaluation.

The DRIVE database comprises 40 eye-fundus color images captured in digital form from a Canon CR5 nonmydriatic 3CCD camera at 45 field of view. The images are of size 768×584 pixels, 8 bits per color channel and have a field of view (FOV) of approximately 540 pixels in diameter. The database is divided into two sets: a test set and a training set, each of them containing 20 images. The test set provides the corresponding FOV masks for the images, in which two manual segmentations are generated by two different specialists for each image. The selection of the first observer is accepted as a ground truth and used for performance evaluation of algorithms in literature. The training set also includes the FOV masks for the images and a set of manual segmentations made by the first observer.

The STARE database comprises 20 eye-fundus color images captured with a TopCon TRV-50 fundus camera at 45° FOV. The images were digitalized to 700×605 pixels, 8 bits per color channel and are available in PPM[33] format. The database contains two sets of manual segmentations made by two different observers. Performance is computed with segmentations of the first observer as ground truth.
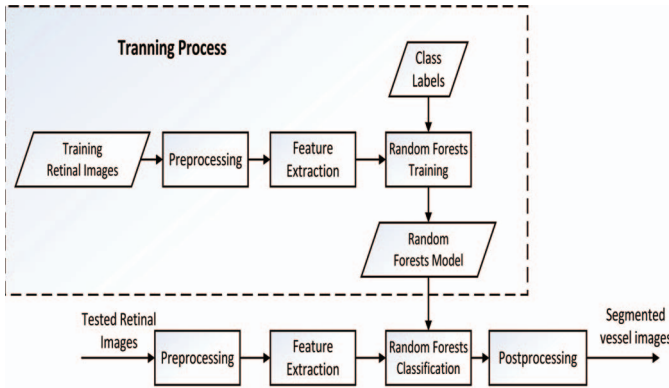

Fig. 1. Overall architecture of vessel segmentation

III. METHOD

In this paper, a new supervised approach is proposed for blood vessel segmentation based on integral channel features and random forests. The proposed method mainly consists of the following process stages: 1) original fundus image preprocessing to obtain candidate pixels which may belong to vessels, 2) feature extraction for each candidate pixel, 3) application of a classifier to label the pixel as vessel or non-vessel, 4) postprocessing for filling pixel gaps in detected blood vessels. The architecture of our process stages is summarized in Fig.1.
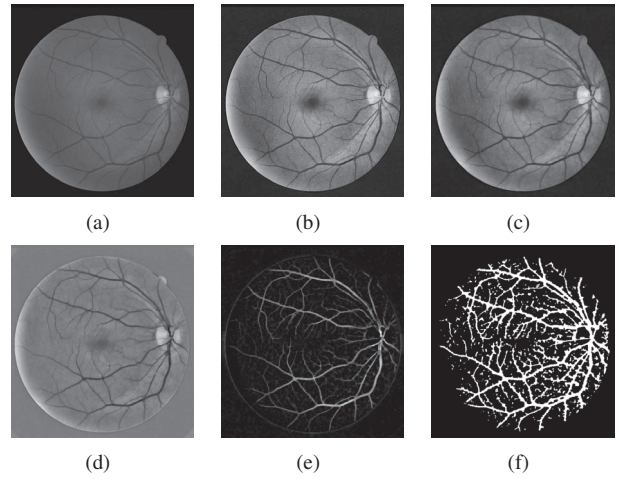

Fig. 2. Illustration of preprocessing process: (a) Green channel of the original image I_g. (b) Vessel-background enhanced image I_{CI}. (c) Image after removing vessel central light reflex I_R (d) Homogenized image I_H. (e) Vessel-enhanced image I_{VE}. (f) Vessel-candidates image I_{cand}.

A. Preprocessing

To reduce the burden of the classifier, the candidate pixels, which may belong to the vessels, are extracted first. Extraction of candidate pixels can be done by the following steps:

First, the green plane of the image I_g [Fig.2.(a)] is processed by applying local histogram equalization with 64 tiles. I_{CI} [Fig.2.(b)] denotes the resultant image for future references.

Secondly, the image I_{CI} is filtered by applying a morphological opening using a three-pixel diameter disc aiming to remove the vessel central light reflex. I_R [Fig.2.(c)] represents the image after removing vessel central light reflex.

Next, with the purpose of removing the background lightening variations, the homogenized image I_H [Fig.2.(d)] is produced according to the following gray-level global transformation function

$$I_H = \begin{cases} 0 & \text{if } I_g < 0 \\ 255 & \text{if } I_g > 255 \\ I_g & otherwise \end{cases} \tag{1}$$

where

$$I_{SC} = I_R - I_B \tag{2}$$

$$I_g = I_{SC} + 128 - I_{SC\_Max} \tag{3}$$

The variable denoted by I_B is produced by applying a 69×69 mean filter mean filter. I_{SC} represents the difference bwtween I_R and I_B and I_{SC_Max} defines the highest number of pixels in I_{SC}

Furthermore, a new vessel-enhanced image I_{VE} [Fig.2.(e)] is produced by estimating the complementary image of the homogenized image I_H, I_H^c, and subsequently applying the morphological Top-Hat transformation

$$I_{VE} = I_H^c - \gamma(I_H^c) \tag{4}$$

(a)   (b)   (c)

(d)   (e)   (f)
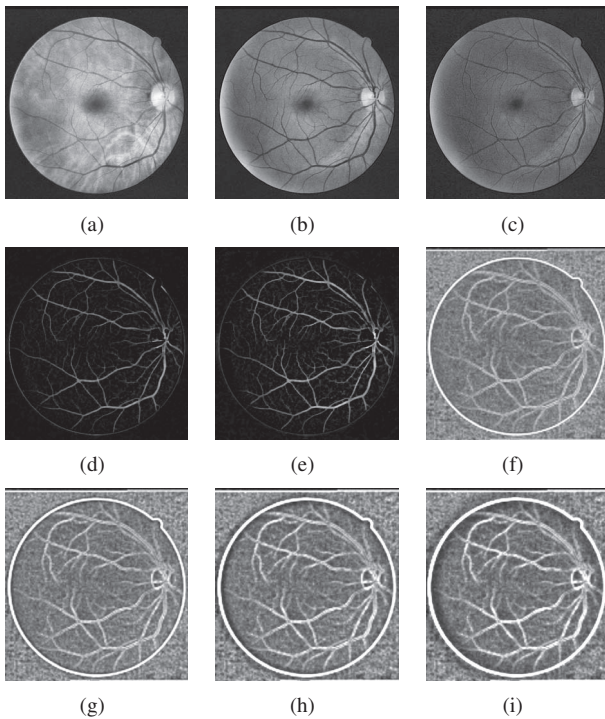
(g)   (h)   (i)

Fig. 3. Computed image channels:(a) Red plane of the image after applying local histogram equalization. (b) Green plane of the image after applying local histogram equalization. (c) Blue plane of the image after applying local histogram equalization. (d) Preprocessing image without local histogram equalization. (e) Preprocessing image with local histogram equalization. (f) Gradient magnitude of the image with 5 normalization radius. (g) Gradient magnitude of the image with 10 normalization radius. (h) Gradient magnitude of the image with 15 normalization radius. (i) Gradient magnitude of the image with 20 normalization radius.

where γ is a morphological opening operation using a disc of eight pixels in radius.

Finally, most of the blood vessel candidates I_{cand} [Fig.2.(f)] are selected with a soft threshold th_{cand}, which is the product of 0.3 (chosen by empirical study) and the global threshold obtained by using Otsus method[32].

B. Feature Extraction

The aim of the feature extraction stage is pixel characterization by means of a feature vector, a pixel representation in terms of some quantifiable measurements which will be used in the classification stage to decide whether a pixel belongs to a real blood vessel or not.

Regarding supervised methods [1,3,4,8,9], lots of different features are designed manually. These features are a culmination of years of effort, and are proven to be effective for vessel segmentation in fundus images. Nevertheless, in this paper, we utilize a simple way to extract features for each candidate pixel. Surprisingly, the competitive results obtained by the proposed method illustrate that such a simple method is effective. The inspiration of the method comes from [5], where integral channel features are presented.

The idea behind integral channel features is that multiple registered image channels are computed using linear and non-linear transformations of the input image, and then the

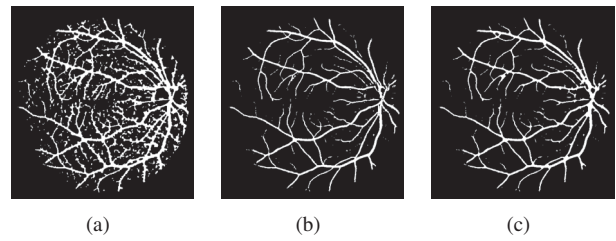
(a)   (b)   (c)

Fig. 4. (a) Vessel-candidates image. (b) Classified image. (c) Postprocessing image.

features such as local sums, histograms, and Haar features and their various generalizations are efficiently computed using integral images [5]. In this paper, we employ the integral channels, and then patch-based method is applied to extract abundant features for each candidate pixel.

1) Transform of Multiple Registered Image Channels: Multiple registered image channels are computed using linear and non-linear transformations of the input image. In this paper, the computed image channels are listed as follows:

- Enhanced RGB Color Channels: Three color channels, red, green and blue channel, are utilized at first. Each color channel is processed by applying local histogram equalization whose number of tiles is equal to 64 in order to enhance the contrast of vessel and background, which generates a more suitable channel for further features extraction. Enhanced RGB color channels are shown in Fig.3. (a), (b) and (c).

- Preprocessed Image Channels: Since preprocessed images reduce the imperfections of color fundus images, they are fixed to extract informative features. Thus two processing images, where one is applied by local histogram equalization(LHE) with 64 tiles and one without LHE, are utilized in our work. Preprocessing image channels are shown in Fig.3. (d) and (e).

- Gradient Magnitude Channels: Gradient magnitude channel can capture unoriented edge strength[5]. The gradient is computed on the red, green and blue color channels separately and the maximum response is chosen[10]. In this work gradients are computed at normalization radius $5, 10, 15$ and 20. Fig.3. (f), (g) and (h), (i), show the gradient magnitude channels.

2) Channel Feature Extraction: After transforming multiple image channels, channel features are extracted at 9 integral image channels, calculated over an image patch with size $m \times n$ pixels. For each pixel representation, $m \times n \times 9$ generic features are obtained. It is notable that there is no need to optimize the feature set in this work.

C. Classification

In the classification stage, since random forests[11−12] can deal with large amounts of high dimensional data rapidly, it is applied to assign one of the classes Y1(vessel) or Y2(nonvessel) to each candidate pixel.

Table I   The experimental results of parameter setting on DRIVE database

The path size	Utilized feature numbers of each node in random forests	The number of trees	Se	Sp	Acc
4 × 4	12	20	0.7005	0.9860	0.9608
	12	5	0.7007	0.9855	0.9604
	12	10	0.6999	0.9860	0.9607
	12	40	0.6986	0.9862	0.9608
	12	80	0.6975	0.9864	0.9609
	3	20	0.6249	0.9867	0.9550
	6	20	0.6721	0.9867	0.9590
	24	20	0.7141	0.9847	0.9608
	48	20	0.7166	0.9844	0.9607
8 × 8	24	20	0.7128	0.9855	0.9614
	24	5	0.7264	0.9823	0.9597
	24	10	0.7187	0.9842	0.9608
	24	40	0.7080	0.9862	0.9616
	24	80	0.7037	0.9865	0.9616
	6	20	0.6438	0.9872	0.9570
	12	20	0.6950	0.9867	0.9610
	48	20	0.7165	0.9852	0.9615
	96	**20**	**0.7191**	**0.9849**	**0.9614**
16 × 16	48	20	0.7085	0.9858	0.9613
	48	5	0.7261	0.9820	0.9594
	48	10	0.7172	0.9843	0.9607
	48	40	0.7024	0.9866	0.9615
	48	80	0.6966	0.9870	0.9614
	12	20	0.6789	0.9866	0.9595
	24	20	0.7019	0.9859	0.9608
	96	20	0.7123	0.9856	0.9615
	192	20	0.7160	0.9852	0.9615

Random forests(RF) are ensembles of m binary decision trees $f_t(x)$: $X \rightarrow Y$, where $X = R^n$ is n-dimensional feature space and $Y = \{Y1 = 1, Y2 = 0\}$ describes the label space[1].

During testing, each decision tree returns a class label probability distribution $p_t(y|x)$ for a given test sample x, and the final class label y^* is calculated via

$$y^* = \underset{y}{\mathrm{argmax}} \frac{1}{m} \sum_{t=1}^{m} p_t(y|x) \qquad (5)$$

During training the decision trees are provided with training data $\mathcal{T} = (x_i, y_i)_{i=1}^{N}$, where N is the number of training examples, and all trees are trained independently. To train a single decision tree, the parameters Θ of a splitting function

$$\Phi(x, \Theta) = \begin{cases} 0 & \text{if } r_\Theta(x) < 0 \\ 1 & \text{otherwise} \end{cases} \qquad (6)$$

have to be estimated, which separates the data into two disjoint sets. In (6), $r_\Theta(x) \rightarrow R$ calculates a response of the feature vector x. The quality of a given splitting function Φ is typically defined as

$$I(\Theta) = \frac{|L|}{|L| + |R|} H(L) + \frac{|R|}{|L| + |R|} H(R) \qquad (7)$$

where $L = \{x : \Phi(x, \Theta) = 0\}$, $R = \{x : \Phi(x, \Theta) = 1\}$, $|\cdot|$ denotes the size of a set, and $H(\cdot)$ measures the purity of a set of training examples in terms of class labels. The

[1]Please note that we only consider the binary case here as our application is binary object detection. In general, RF are inherently multi-class.

purity $H(\cdot)$ is typically calculated via the entropy or the Gini index[11].

The standard procedure in Random Forests for finding a good splitting function in a single node is to randomly sample a set of parameters $\{\Theta_j\}_{j=1}^{k}$ and simply choosing the best one, Θ^*, by evaluating (7). This splitting function is then fixed, and the trees continues growing until some stop criteria, such as a maximum tree depth or a minimum numbers of samples in the node, are reached.

The classified image corresponding to a vessel candidate image [Fig.4.(a)] is shown in Fig.4.(b).

D. Postprocessing

From visual inspection of the image in Fig.4.(b), the vessels still have a few gaps. To overcome this problem, the detected image is filtered by a morphological opening using a three-pixel diameter diamond. The final image after this post processing is shown in Fig.4.(c).

IV. EXPERIMENTAL RESULTS

A. Parameter setting

The proposed algorithm was evaluated in terms of sensitivity (Se), specificity (Sp) and accuracy (Acc). Let TP means true positive, TN true negative, FP false positive and FN false negative. These metrics are defined as:

$$Se = TP/(TP + FN) \qquad (8)$$
$$Sp = TN/(TN + FP) \qquad (9)$$
$$Acc = (TP + TN)/(TP + TN + FP + FN) \qquad (10)$$

Se and Sp metrics are the ratio of well-classified vessel to nonvessel pixels, respectively. Acc is a global measure providing the ratio of well-classified pixels to all pixels.

In our work, three crucial parameters, patch size, number of utilized features of each node in RF and number of trees, need to design carefully. To evaluate the effects of the parameters for the algorithm, we tested the algorithm on the DRIVE database, in which test set and training set are separated. The experimental results of parameter setting are shown in Table I. It can be observed that when the patch size and the number of trees are fixed, increasing the number of utilized features of each node in RF improves the Se and Acc, but deteriorates Sp. When the patch size and the number of utilized features of each node in RF are fixed, increasing the number of trees improves the Sp and Acc, but deteriorates Se.

To facilitate the validation of the proposed method on STARE databases and comparing it with other algorithms, we fixed all parameters before testing. According to the analysis of Table I, the patch size as 8×8, the number of utilized features of each node as 96 and number of trees as 20 are the good choices, neither too small to lose the performance nor too large to increase the unnecessary computation. The performance results are shown in Table II and Table III. Note that there are no specified training images for STARE database, thus we utilized the classifier trained on DRIVR training images to test the method on STARE images.

B. Comparison to other methods

Through previous experiments the proposed method has been demonstrated to be effective and efficient for vessel segmentation. In order to emphasize the effectiveness of our method, we compare our model with other existing state-of-the-art vessel detection methods on the two most popular public databases: the DRIVE database and the STARE database. Table IV and Table V show the performance comparison of our method and the others on both the DRIVE and STARE databases in terms of Se, Sp and Acc, respectively, with the following published methods: Ricci *et al.*[3], Marin *et al.*[4], Hoover *et al.*[6], Niemeijier *et al.*[7], Soares *et al.*[8], Staal *et al.*[9], Orlando *et al.*[13], Wang *et al.*[14], Lupascu *et al.*[15], Fraz *et al.*[16], Zana *et al.*[17], Al-Diri *et al.*[18], Budai *et al.*[19], Lam *et al.*[20], Nguyen *et al.*[21], You *et al.*[22], Mendonca *et al.*[23], Perez *et al.*[24], Jiang *et al.*[25]. The values shown in each table are presented for each database as reported by their authors. If they are not available for a specific database or not calculated for the 20 images selected for testing, they were not included in the tables, thus appearing as gaps.

From Table IV, we observe that the proposed vessel segmentation algorithm out performs other existing methods on the DRIVE test data set in terms of segmentation Acc, and $Sp = 0.985$, which is only 0.002 lower than the method proposed by Budai *et al.*[19]. Although one of the supervised method [13] has a higher sensitivity, it has a much lower specificity than most of the other methods. Similarly, from Table V, the proposed method proves useful for vessel

Table II   Performance results on DRIVE database images

Image	Se	Sp	Acc
1	0.7918	0.9803	0.9634
2	0.7792	0.9852	0.9641
3	0.6379	0.9914	0.9561
4	0.7293	0.9880	0.9642
5	0.6608	0.9909	0.9599
6	0.6242	0.9919	0.9561
7	0.7279	0.9804	0.9573
8	0.6440	0.9881	0.9585
9	0.5856	0.9939	0.9609
10	0.7112	0.9867	0.9640
11	0.7502	0.9790	0.9585
12	0.7412	0.9853	0.9642
13	0.6877	0.9879	0.9585
14	0.7835	0.9772	0.9616
15	0.8089	0.9682	0.9568
16	0.7115	0.9872	0.9623
17	0.6666	0.9890	0.9618
18	0.7449	0.9827	0.9638
19	0.8335	0.9818	0.9695
20	0.7620	0.9834	0.9671
Average	**0.7191**	**0.9849**	**0.9614**

Table III   Performance results on STARE database images

Image	Se	Sp	Acc
1	0.5835	0.9859	0.9538
2	0.5646	0.9881	0.9599
3	0.7884	0.9661	0.9554
4	0.2607	0.9972	0.9426
5	0.8176	0.9550	0.9426
6	0.8423	0.9675	0.9588
7	0.9017	0.9579	0.9534
8	0.9028	0.9646	0.9600
9	0.7879	0.9846	0.9691
10	0.7968	0.9608	0.9476
11	0.8276	0.9785	0.9678
12	0.8597	0.9795	0.9703
13	0.8117	0.9764	0.9618
14	0.8248	0.9778	0.9640
15	0.7838	0.9794	0.9625
16	0.6111	0.9874	0.9490
17	0.8377	0.9782	0.9656
18	0.6444	0.9946	0.9769
19	0.2926	0.9978	0.9674
20	0.2529	0.9967	0.9470
Average	**0.6996**	**0.9787**	**0.9588**

Table IV   Performance comparison of vessel segmentation methods on DRIVE database

Method Type	Methods	Se	Sp	Acc
Supervised	Niemeijier *et al.*[7]	–	–	0.942
	Staal *et al.*[9]	–	–	0.944
	Orlando *et al.*[13]	0.785	0.967	–
	Wang *et al.*[14]	–	–	0.946
	Lupascu *et al.*[15]	0.720	–	0.960
	Marin *et al.*[4]	0.707	0.980	0.945
	Ricci *et al.*[3]	–	–	0.960
	Fraz *et al.*[2]	0.741	0.981	0.948
	Proposed Method	**0.719**	**0.985**	**0.961**
Other	Zana *et al.*[17]	0.697	–	0.938
	Al-Diri *et al.*[18]	0.728	0.955	–
	Budai *et al.*[19]	0.644	0.987	0.957
	Fraz *et al.*[16]	0.715	0.976	0.943
	Lam *et al.*[20]	–	–	0.947
	Nguyen *et al.*[21]	–	–	0.941

Table V   Performance comparison of vessel segmentation methods on STARE database

Method Type	Methods	Se	Sp	Acc
Supervised	Staal *et al*.[9]	–	–	0.952
	Soares *et al*.[8]	0.721	0.975	0.946
	Ricci *et al*.[3]	–	–	0.952
	Marin *et al*.[4]	0.694	0.982	0.953
	Wang *et al*.[14]	–	–	0.952
	You *et al*.[22]	0.726	0.975	0.949
	Proposed Method	**0.700**	**0.979**	**0.959**
Other	Mendonca *et al*.[23]	0.699	0.973	0.944
	Fraz *et al*.[16]	0.731	0.968	0.944
	Nguyen *et al*.[21]	–	–	0.932
	Al-Diri *et al*.[18]	0.752	0.968	–
	Perez *et al*.[24]	0.769	0.944	0.926
	Lam *et al*.[20]	–	–	0.947
	Hoover *et al*.[6]	0.675	0.957	0.926
	Jiang *et al*.[25]	–	–	0.901

detection in STARE images. Its application to this database results in the highest accuracy score and the second highest specificity score among all methods(only behind Marin's approach [4]).

V. DISCUSSION AND CONCLUSION

In this paper, we propose a new supervised retinal blood vessel segmentation method, which is based on integral channel features and random forests. With the aim of minimizing the human effort of designing and implementing features, integral channel features are extracted from multiple registered image channels, which are computed using linear and non-linear transformations of the input image. Then random forests is applied to label the pixels as vessel or non-vessel. The results(Se of 0.7190, Acc of 0.9850 and Sp of 0.9610 on DRIVE database, Se of 0.700, Acc of 0.9790 and Sp of 0.9590 on STARE database) manifest that the method is effective for vessel segmentation. Next we plan to apply our method to other biomedical images, e.g. membrane segmentation.

REFERENCES

[1] Roychowdhury S, Koozekanani D, Parhi K. Blood vessel segmentation of fundus images by major vessel extraction and sub-image classification. *Biomedical and Health Informatics*, 2014, 19(3): 1118−1128

[2] Fraz M M, Remagnino P, Hoppe A. Blood vessel segmentation methodologies in retinal images−A survey. *Computer Methods and Programs in Biomedicine*, 2012, 108(1): 407−433

[3] Ricci E, Perfetti R. Retinal blood vessel segmentation using line operators and support vector classification. *IEEE Transactions on Medical Imaging*, 2007, 26(10): 1357−1365

[4] Marin D, Aquino A, Gegundez-Arias M E. A new supervised method for blood vessel segmentation in retinal images by using gray-level and moment invariants-based features. *IEEE Transactions on Medical Imaging*, 2011, 30(1): 146−158

[5] Dollr P, Tu Z, Perona P. Integral channel features. In: Proceedings of British Machine Vision Conference. London, UK: BMVA, 2009. 5−5.

[6] Hoover A, Kouznetsova V, Goldbaum M. Locating blood vessels in retinal images by piecewise threshold probing of a matched filter response. *IEEE Transactions on Medical Imaging*, 2000, 19(3): 203−210

[7] Niemeijer M, Staal J, van Ginneken B. Comparative study of retinal vessel segmentation methods on a new publicly available database. In: Proceedings of SPIE Medical Imaging. San Diego, USA: SPIE, 2004. 648−656.

[8] Soares J V B, Leandro J J G, Cesar Jr R M. Retinal vessel segmentation using the 2-D Gabor wavelet and supervised classification. *IEEE Transactions on Medical Imaging*, 2006, 25(9): 1214−1222

[9] Staal J, Abrmoff M D, Niemeijer M. Ridge-based vessel segmentation in color images of the retina. *IEEE Transactions on Medical Imaging*, 2004, 23(4): 501−509

[10] Dalal N, Triggs B. Histograms of oriented gradients for human detection. In: Proceedings of Computer Vision and Pattern Recognition. Washington, USA: IEEE, 2004. 886−893

[11] Breiman L. Random forests. *Machine learning*, 2001, 45(1): 5−32

[12] Mitchell T. Machine Learning. McGraw-Hill, 1997

[13] Orlando J I, Blaschko M. Learning Fully-Connected CRFs for Blood Vessel Segmentation in Retinal Images. *Lecture Notes in Computer Science*, 2014, 17: 634−641

[14] Wang Y, Ji G, Lin P. Retinal vessel segmentation using multiwavelet kernels and multiscale hierarchical decomposition. *Pattern Recognition*, 2013, 46(8): 2117−2133

[15] Lupascu C A, Tegolo D, Trucco E. FABC: retinal vessel segmentation using AdaBoost. *IEEE Transactions on Information Technology in Biomedicine*, 2010, 14(5): 1267−1274

[16] Fraz M M, Barman S A, Remagnino P. An approach to localize the retinal blood vessels using bit planes and centerline detection. *Computer Methods and Programs In Biomedicine*, 2012, 108(2): 600−616

[17] Zana F, Klein J C. Segmentation of vessel-like patterns using mathematical morphology and curvature evaluation. *IEEE Transactions on Medical Imaging*, 2001, 10(7): 1010−1019

[18] Al-Diri B, Hunter A, Steel D. An active contour model for segmenting and measuring retinal vessels. *IEEE Transactions on Medical Imaging*, 2009, 28(9): 1488−1497

[19] Budai A, Bock R, Maier A. Robust vessel segmentation in fundus images. *International journal of biomedical imaging*, 2013, 2013: 154860−154860

[20] Lam B S Y, Gao Y, Liew A W C. General retinal vessel segmentation using regularization-based multiconcavity modeling. *IEEE Transactions on Medical Imaging*, 2010, 29(7): 1369−1381

[21] Nguyen U T V, Bhuiyan A, Park L A F. An effective retinal blood vessel segmentation method using multi-scale line detection. *Pattern recognition*, 2013, 46(3): 703−715.

[22] You X, Peng Q, Yuan Y. Segmentation of retinal blood vessels using the radial projection and semi-supervised approach. *Pattern recognition*, 2011, 44(10): 2314−2324.

[23] Mendonca A M, Campilho A. Segmentation of retinal blood vessels by combining the detection of centerlines and morphological reconstruction. *IEEE Transactions on Medical Imaging*, 2006, 25(9): 1200−1213

[24] Palomera-Prez M A, Martinez-Perez M E, Benłtez-Prez H, et al. Parallel multiscale feature extraction and region growing: application in retinal blood vessel detection. *IEEE Transactions on Information Technology in Biomedicine*, 2010, 14(2): 500−506.

[25] Jiang X, Mojon D. Adaptive local thresholding by verification-based multithreshold probing with application to vessel detection in retinal images. *IEEE Transactions on Pattern Analysis and Machine Intelligence*, 2003, 25(1): 131−137.

[26] Zhang B, Zhang L, Zhang L. Retinal vessel extraction by matched filter with first-order derivative of Gaussian. *Computers in biology and medicine*, 2010, 40(4): 438−445.

[27] Amin M A, Yan H. High speed detection of retinal blood vessels in fundus image using phase congruency. *Soft Computing*, 2011, 15(6): 1217−1230.

[28] Delibasis K K, Kechriniotis A I, Tsonos C. Automatic model-based tracing algorithm for vessel segmentation and diameter estimation. *Computer methods and programs in biomedicine*, 2010, 100(2): 108−122.

[29] Miri M S, Mahloojifar A. Retinal image analysis using curvelet transform and multistructure elements morphology by reconstruction. *IEEE Transactions on Biomedical Engineering*, 2011, 58(5): 1183−1192.

[30] Farnell D J J, Hatfield F N, Knox P. Enhancement of blood vessels in digital fundus photographs via the application of multiscale line operators. *Journal of the Franklin institute*, 2008, 345(7): 748−765.

[31] Vlachos M, Dermatas E. Multi-scale retinal vessel segmentation using line tracking. *Computerized Medical Imaging and Graphics*, 2010, 34(3): 213−227.

[32] Otsu N. A threshold selection method from gray-level histograms. *Automatica*, 1975, 11(285-296): 23-27.

[33] PPM[Online], available: http://netpbm.sourceforge.net/doc/ppm.html, Janurary 15, 2016.